



# Experiments on coherent adaptive antenna array diversity for wideband DS-CDMA mobile radio

著者	安達 文幸
journal or publication title	IEEE Journal on Selected Areas in Communications
volume	18
number	8
page range	1495-1504
year	2000
URL	<a href="http://hdl.handle.net/10097/46426">http://hdl.handle.net/10097/46426</a>

doi: 10.1109/49.864013

# Experiments on Coherent Adaptive Antenna Array Diversity for Wideband DS-CDMA Mobile Radio

Shinya Tanaka, Atsushi Harada, Mamoru Sawahashi, *Member, IEEE*, and Fumiyuki Adachi, *Senior Member, IEEE*

**Abstract**—In wideband direct sequence code division multiple access (W-CDMA), employing an adaptive antenna array is a very promising technique to reduce severe multiple access interference (MAI) from high rate users. A four-antenna pilot symbol-assisted coherent adaptive antenna array diversity (PSA-CAAAD) receiver comprising an adaptive antenna array based on a minimum mean squared error (MMSE) criterion and a Rake combiner is implemented in preliminary laboratory and field experiments. There are two important design concepts of the PSA-CAAAD receiver. The first is that the adaptive antenna array forms an antenna beam for each resolved propagation path and tracks only slow changes in the directions of arrival (DOA's) and average powers of the desired and interfering user signals. The second is that the Rake combiner tracks the instantaneous changes in channel conditions and coherently combines the signals of the desired user propagating along the resolved paths to maximize the instantaneous signal-to-interference plus background noise power ratio (SINR). This paper presents, both by laboratory and field experiments, the effectiveness of PSA-CAAAD receiver as a powerful means to reduce severe MAI from high rate users, and that it is more effective than using a space diversity receiver with the same number of antennas in the W-CDMA reverse link.

**Index Terms**—Adaptive antenna array, DS-CDMA, mobile communications.

## I. INTRODUCTION

WIDEBAND direct sequence code division multiple access (wideband DS-CDMA or W-CDMA) [1], [2] has been accepted as a wireless access scheme for IMT-2000 [3]. In DS-CDMA, all users communicate simultaneously in the same frequency band and, hence, multiple access interference (MAI) is the major cause of transmission impairment. In mobile radio, since the received signal is subject to multipath fading according to the movement of a mobile terminal, in addition to distance-dependent path loss and shadowing, a high degree of MAI is often produced, which significantly degrades the reverse link performance. However, in multimedia mobile communications offered by, for example, the IMT-2000 system, data rates may vary widely and high rate users may produce severe MAI in the reverse (mobile-to-base) link. A promising technique to reduce the severe MAI from high rate users is employing an adaptive antenna array [4]–[9].

In [17], the optimum combining (i.e., adaptive antenna array diversity) that maximizes the output of signal-to-interference

plus background noise ratio (SINR) with cochannel interference was presented, and optimum combining was shown to be significantly better than maximal ratio combining (MRC) even when the number of interfering users is greater than that of antennas. We recently proposed the pilot symbol-assisted coherent adaptive antenna array diversity (PSA-CAAAD hereafter) receiver [10] that combines an adaptive antenna array and a Rake combiner. Basically our approach is the same as that in [17] in that the receiver antenna weights are adaptively controlled so that the SINR is maximized. However, our approach is different from their method in the following two points. First, in [17], the antennas are spaced far enough apart so that the fading seen on each antenna is independent. This means that coherent channel estimation needs to be done before combining, i.e., before interference suppression. Therefore, a large channel estimation error may occur under low SINR conditions. On the other hand, we assume a linear array with the antenna separation of half a carrier wavelength. Since the fading seen on each antenna can be assumed identical, the received signal combining is performed first and, then, channel estimation is done after interference suppression, thereby decreasing the channel estimation error. Second, the design concept of beam forming is different. In a conventional adaptive antenna array diversity receiver with the antenna separation of half a carrier wavelength similar to our approach, the receiver antenna weights are generated to maximize the instantaneous SINR using an adaptive algorithm [20]. Our final objective is to develop the adaptive antenna array receiver and transmitter, in which the generated receiver antenna weights are used to generate transmit antenna beams on the forward link, so that the adaptive antenna array receiver and transmitter can be equipped at a base station. However, since frequency division duplex (FDD) is used in the W-CDMA systems, the instantaneous phase and amplitude variations due to fading in the reverse link have no correlation to those in the forward link. Noting that the distance-dependent macroscopic propagation factors determining the average signal power, i.e., path loss and shadowing, are not frequency dependent, we design the PSA-CAAAD receiver based on the following concept. The adaptive antenna array forms an antenna beam that tracks only slow changes in the directions of the arrival (DOA's) and average powers of the desired and interfering users, and the Rake combiner tracks the instantaneous variations in the channel conditions to maximize the instantaneous SINR. However, note that in this paper we only consider the adaptive antenna array receiver.

This paper presents, both by laboratory and field experiments, the effectiveness of the PSA-CAAAD receiver in the reverse link (or uplink) for DS-CDMA mobile radio. We have already

Manuscript received August 1999; revised February 28, 2000. This paper was presented in part at the first International Symposium on the IEEE Vehicular Technology Conference (VTC) '99, Houston, Texas, U.S.A., May 16–19, 1999. The authors are with the Wireless Laboratories, NTT Mobile Communications Network, Inc., 3-5 Hikari-no-oka, Yokosuka-shi, Kanagawa-ken, 239-8536 Japan (e-mail: stanaka@mlab.yrp.nttdocomo.co.jp).  
Publisher Item Identifier S 0733-8716(00)06116-3.

TABLE I  
RADIO LINK PARAMETERS

Chip rate (Bandwidth)		4.096 Mcps (5 MHz)
Carrier frequency (Reverse)		1990.5 MHz
Symbol rate		64 ksp/s
Spreading factor		64
Information bit rate		32 kbps
Spreading code	Short code	Orthogonal-Gold sequence (64 chips)
	Scrambling code	Truncated-Gold sequence ( $640 \times 2^{29}$ chips)
Modulation	Data	QPSK
	Spreading	QPSK
Channel estimation for coherent detection		Pilot symbol-assisted channel estimation (2-slot averaging)
Channel coding and decoding		Convolutional coding ( $R=1/3$ , $k=7$ ) Soft-decision Viterbi decoding
Interleaving size		10 ms

shown the preliminary experimental results using the adaptive antenna with only 2 antennas in [15]. In this paper, a great deal of detailed laboratory and field experimental results are presented for the generated beam patterns and the average bit error rate (BER) performance in various conditions using a four-antenna PSA-CAAAD receiver. The experimental results show that combining the adaptive antenna array and Rake combiner is a powerful means to reduce severe MAI from high rate users and is more effective than using a space diversity receiver with the same number of antennas. In this paper, we first describe, in Section II, a four-antenna PSA-CAAAD receiver implemented for 5 MHz W-CDMA for use in preliminary laboratory and field experiments. Sections III and IV discuss the beam patterns and the measured average BER performance obtained from laboratory and field experiments, respectively.

## II. EXPERIMENTAL PSA-CAAAD RECEIVER

### A. Overall Receiver Structure

The major radio link parameters of the experimental four-antenna PSA-CAAAD receiver are listed in Table I, which is based on [18]. The transmission bit rate is 32 kbit/s, and the channel coding is a 1/3-rate convolutional code with a constraint length of 7 bits. The coded data were block interleaved and then transformed into a quaternary phase shift keyed (QPSK) symbol sequence. There were four pilot symbols appended to every set of 36 data symbols to form one slot. Each 10-ms frame comprised 16 slots of 0.625 ms each (each slot comprised 40 symbols). The resultant QPSK symbol rate was 64 ksymbol/s. The QPSK symbol sequence of each data channel was multiplied with an orthogonal-Gold sequence with the repetition period of 64 chips (the spreading factor is  $SF = 64$ ) and a scrambling code with the repetition period of  $640 \times 2^{29}$  chips. The spreading chip rate was 4.096 Mcps/s. To confine the spread signals within the bandwidth of 5.0 MHz, a square-root raised cosine Nyquist transmit filter with the rolloff factor of 0.22 was applied before frequency conversion into the carrier frequency of 1990.5 MHz and power amplification. Note that the radio link parameters used in the paper are different from that of the latest standard in 3rd Generation Partnership Project (3GPP) [19]. In the latest

3GPP standard, the chip rate is 3.84 Mcps/s and one frame comprises 15 slots, the length of each is 0.667 ms. The scrambling code length on the reverse link is 38 400 chips ( $=10$  ms in time). The pilot symbols on the reverse link to be used for coherent channel estimation is multiplexed onto the quadrature (Q) channel while the coded data symbols are multiplexed onto the in-phase (I) channel. Since the difference in the slot lengths is small (0.667 ms against 0.625 ms), the impact on the tracking performance of channel estimation and fast TPC against fading is considered very small. Furthermore, the impact of the difference in the pilot symbol structure (I/Q code-multiplexed against time multiplexed) on the channel estimation is also considered small because almost the same pilot power is assigned per slot. Thus, the obtained results in the paper can be applied to the latest 3GPP air interface.

A block diagram of the experimental PSA-CAAAD receiver is illustrated in Fig. 1. The composite spread signal received on each antenna was converted into baseband I and Q components by a quadrature detector. They were sampled at the rate of  $4 \times 4.096$  MHz using an 8-bit A/D converter. After being filtered using a square-root raised cosine Nyquist filter, the sampled signals were fed into the PSA-CAAAD processing block, which outputs the QPSK soft decision sample sequence that corresponds to the transmitted coded interleaved binary data sequence. After deinterleaving, soft decision Viterbi decoding was applied to recover the transmitted data.

### B. PSA-CAAAD Processing Block

The PSA-CAAAD processing block structure is illustrated in Fig. 2. It comprises digital matched filters (MF's), a digital beam former, PSA-coherent Rake combiner, and antenna weight controller. The sequence of the filtered received signal samples was first despread by the MF's and resolved into multiple copies of the transmitted QPSK symbol sequence that were propagated along different propagation paths. The propagation channel comprises many paths with different time delays. The paths within one chip time length are seen as a single composite path at the receiver MF output and cannot be separable or resolvable (this is because the time resolution of the MF is one chip time). Therefore, in the laboratory experiment, we modeled the propagation channel as the sum of several resolvable paths with a time delay difference between adjacent paths such that it is more than one chip length ( $=0.24 \mu\text{s} = 1/4.096$  Mcps/s). The MF's were implemented as a bank of correlators, each comprising a multiplier and an integrate-and-dump (I&D) filter. In each MF, the received signal was first multiplied with a locally generated spreading code replica in which the timing was locked to the measured time delay of each of the resolvable propagation paths, and then integrated by the I&D filter over the QPSK symbol interval. Path search for Rake combining was conducted based on the average power delay profile. First, the instantaneous power delay profile per slot was measured by coherently averaging the MF output belonging to 4 pilot symbols. Then, by averaging the instantaneous power delay profile over 100 ms, the average power delay profile was obtained. The choice of the measurement time for the average power delay profile depends on the changing speed of the multipath delay times. However, we found based on the field experiments conducted in Tokyo, in

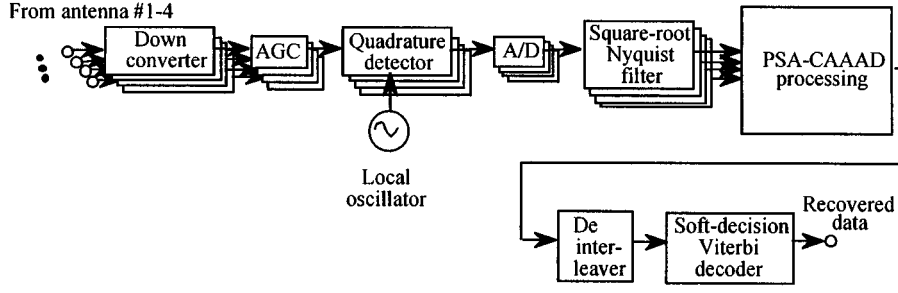


Fig. 1. PSA-CAAAD receiver structure.

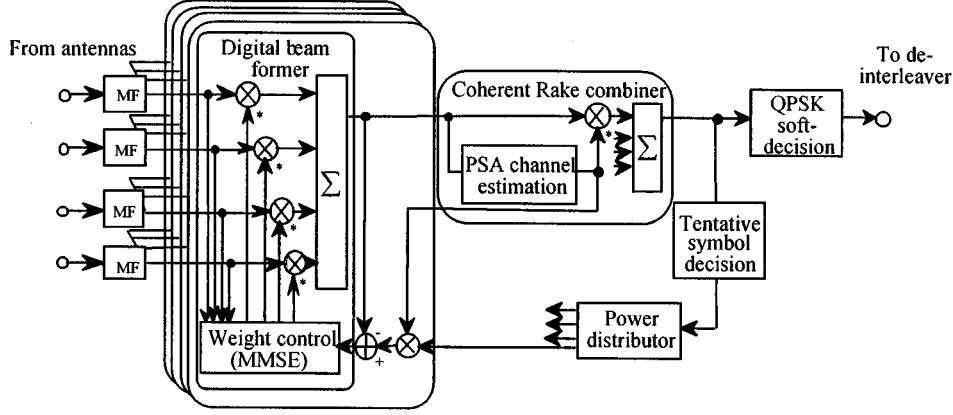


Fig. 2. Block diagram of PSA-CAAAD processing.

which the mobile station was driven at a speed of approximately 30 km/h, that the required received  $E_b/I_0$  was minimized when the average power delay profile measurement time was 100 ms. Therefore, we used 100 ms for the average power delay profile measurement time in the experiments. In our experimental receiver, since the beam pattern was directed toward each path, we used an omnidirectional beam pattern (which is generated by setting one of four weights to 1 and others to 0) for path searching.

Since the distance between both ends of the array antenna is 22 cm for a four-antenna adaptive antenna array, as will be described in Section III, the delay time difference between both ends of the array antenna is a chip duration of only  $3 \times 10^{-3}$ . Therefore, the shapes of the power delay profiles observed at the 4 antennas are still the same, and the timing extraction can be performed using one power delay profile measured at a particular antenna. This timing information was used at the other antennas. The receiver was designed to select three resolvable paths at maximum in decreasing order of the average received power.

The MF output sample  $y_{k,l}^{(j)}(m)$  at time  $t = mT + \tau_{k,l}$  ( $T$  is the QPSK data symbol interval, and  $\tau_{k,l}$  is time delay) associated with the  $k$ th user of the  $l$ th resolved path ( $l = 1, \dots, L_k$ ,  $L_k$  is less than 3) on the  $j$ th antenna ( $j = 1, \dots, 4$ ) is given by

$$y_{k,l}^{(j)}(m) = \frac{1}{T} \int_{mT+\tau_{k,l}}^{(m+1)T+\tau_{k,l}} r^{(j)}(t) p_k^*(t - \tau_{k,l}) dt \quad (1)$$

where  $r^{(j)}(t)$  and  $p_k(t)$  are the received signal on the  $j$ th antenna and the spreading waveform, respectively, and  $*$  denotes

the complex conjugate. In the beam former, the despread signal samples  $y_{k,l}^{(j)}(m)$ 's of 4 antennas are weighted and combined to form a receive antenna beam pattern for each resolved path so that the SINR of the combined signal associated with each of  $L_k$  resolved paths can be maximized in the average sense. Since the weight adaptation algorithm is detailed in [10], we briefly explain the process. The resulting  $l$ th signal sample  $z_{k,l}(m)$  (which is the  $l$ th path beam former output) is represented as

$$z_{k,l}(m) = \sum_{j=1}^4 y_{k,l}^{(j)}(m) w_{k,l}^{(j)*}(m) \quad (2)$$

where  $w_{k,l}^{(j)}(m)$  is the weight associated with the  $j$ th antenna. In order to coherently combine the  $L_k$  beam former outputs,  $z_{k,l}(m)$ 's, the resultant composite channel gain (multiplied with rms amplitude) at time  $t = mT + \tau_{k,l}$ , which is given by

$$\eta_{k,l}(m) = \sum_{j=1}^4 \sqrt{2S_{k,l}} \xi_{k,l}^{(j)}(m) w_{k,l}^{(j)*}(m) \quad (3)$$

needs to be estimated using periodically received known pilot symbols [ $S_{k,l}$  and  $\xi_{k,l}^{(j)}$  are the average received signal power and complex channel gain associated with the  $l$ th path of the  $k$ th user].  $\eta_{k,l}(m)$  is estimated using the simple average estimation method [12] with 8 pilot symbols of two succeeding slots as

$$\hat{\eta}_{k,l} = \frac{1}{2} \left( \frac{1}{4} \sum_{m=1}^4 z_{k,l}(m) + \frac{1}{4} \sum_{m=41}^{44} z_{k,l}(m) \right). \quad (4)$$

Using the channel estimate,  $\hat{\eta}_{k,l}$ , the random phase of the  $l$ th beam former output,  $z_{k,l}(m)$ ,  $m = 4, 5, \dots, 40$ , is removed

to be coherently combined by the Rake combiner. The Rake combiner output is given by

$$z_k(m) = \sum_{l=1}^{L_k} z_{k,l}(m) \hat{\eta}_{k,l}^* \quad (5)$$

The receiver antenna weights  $w_{k,l}^{(j)}(m)$  of (2) are updated using the normalized least mean squares (N-LMS) algorithm [11] so that the mean square error (MSE) in the beam former output  $z_{k,l}(m)$  is minimized. For generating reference signal  $\hat{z}_{k,l}(m)$ , required for MSE calculation, the tentative recovered data symbols after coherent Rake combining were used in addition to pilot symbols to establish faster convergence of the antenna weights. The details regarding the generation of  $\hat{z}_{k,l}(m)$  are described in [10]. Then, error signal  $e_{k,l}(m)$  is generated as

$$e_{k,l}(m) = \hat{z}_{k,l}(m) - z_{k,l}(m). \quad (6)$$

Since PSA channel estimation incurs one time slot delay (40 symbols), the error signal associated with the  $m$ th time position of the previous slot is used for weight updating at the  $m$ th time position of the present slot. Consequently, weight vector  $w_{k,l}^{(j)}(m)$  can be updated every 4 symbols as

$$\begin{aligned} w_{k,l}^{(j)}(m+4) \\ = w_{k,l}^{(j)}(m) + \mu \frac{y_{k,l}^{(j)}(m-40)}{\sum_{j=1}^4 |y_{k,l}^{(j)}(m-40)|^2} e_{k,l}^*(m-40) \end{aligned} \quad (7)$$

where  $\mu$  is the step size and was set to  $\mu = 10^{-4}$  in the experiments. Forming a beam null toward the second path with a very different DOA from the first path does not degrade performance. The reason for this is detailed hereafter. Let us assume a 2-path model for simplicity. In our beamforming algorithm, the receiver antenna pattern is formed and updated for each resolvable path. Therefore, for the antenna pattern for the first (second) path, the beam null is generated toward the second (first) path. In this way, the multipath interference on the other path is suppressed and hence, the signal-to-noise ratio on each path is improved. Since the channel estimation using pilot symbols is performed separately for the first and second paths after beam forming, the Rake-combining effect is improved by using our beam forming algorithm.

### III. LABORATORY EXPERIMENTS

In the laboratory experiments, two users (one interfering user) or six users (five interfering users) were considered that transmit continuously at the same data rate (i.e., 32 kb/s) for four-antenna PSA-CAAAD receiver. Assuming the same received quality [measured by BER or frame error rate (FER)], the received signal power (thus, transmit power) must be increased in proportion to the information bit rate. Since the PSA-CAAAD receiver is a single-user type receiver, it does not demodulate the other interfering users' received signals. This means that the received signal quality of the desired user depends only on the received interference power. Instead of using higher rate interfering users, we can simulate the same

condition by using 32 kb/s interfering users but with higher powers, e.g., the interference from a 32 kb/s user with double the transmit power is equivalent to that of a 64 kb/s user requesting the same BER performance. The transmitting timing of each user was asynchronous. Two or six fading simulators were used to simulate multipath signals that follow independent 2-path Rayleigh fading with the maximum Doppler frequency  $f_D = 80$  Hz. The delay time difference between paths was set to  $0.3 \mu\text{s}$  corresponding to a chip length of 1.23. If the time delay difference between two paths is less than one chip length, i.e.,  $0.24 \mu\text{s}$ , they cannot be resolved by the receiver MF and are seen as a single path. If the time difference is longer than one chip length, the paths can be resolved unless the time delay difference is shorter than the scrambling code repetition period, which in our case is  $640 \times 2^{29}$ -chip length, regardless of whether the time delay difference is shorter or longer than the symbol length. In the experiment, therefore, we set the time delay difference to  $0.3 \mu\text{s}$ . Note, however, that the length of the path search window was 2 symbols, i.e.,  $31.25 \mu\text{s}$ , in the implemented receiver.

We assumed a linear array with the separation of half a carrier wavelength. In a real propagation environment, the same faded signal of a certain user that propagates via a certain path may arrive at different antennas with different DOA's. However, in the experiment, we assumed that a macrocell environment with a high-elevation base station array antenna and the mobile station is located at a sufficiently far distance so that the DOA is the same for all antennas. The fading simulator output was divided into four, each of which was phase shifted and combined with other user signals, where the phase shift is given by  $180 \times (j-1) \sin \theta$  degrees for antenna  $\#j$ ,  $j = 1-4$ , with  $\theta$  being the DOA. Finally, Gaussian noise was added to obtain the composite received spread signal at each antenna and was input into the receiver.

First, we measured the antenna beam patterns. The nominal DOA's of the two users were set to  $-50^\circ$  and  $+40^\circ$  for the desired user (User #1) and interfering user (User #2), respectively. The initial antenna weights were set to 1.0 for one antenna and 0 for the others. The converged beam pattern associated with two resolved paths of User #1 is plotted in Fig. 3 for two angle deviations,  $\alpha$ , of two paths from the nominal DOA ( $+\alpha$  degrees for one path and  $-\alpha$  degrees for the other). When the 2 paths are received with the same time delay but from different incident angles, the Rake receiver cannot resolve them. Therefore, the beam pattern that has the main lobes directed toward the 2 paths is generated. In this paper, however, we only consider the case in which paths with different incident angles have different time delays. We computed the beam pattern from the actually generated receiver antenna weights. Since the antenna beam pattern is formed at the baseband processor, the generated antenna weights are affected by the phase and amplitude variations among the four RF circuits (from low-noise amplifier to A/D converters). To correctly illustrate the antenna beam pattern at the receiver input, the RF circuitry's phase and amplitude variations must be removed from the generated antenna weights. To do this, we measured the phase and amplitude variations by applying the test signal at the receiver input and measuring the amplitude and phase of each RF circuit. In the field experiment, the

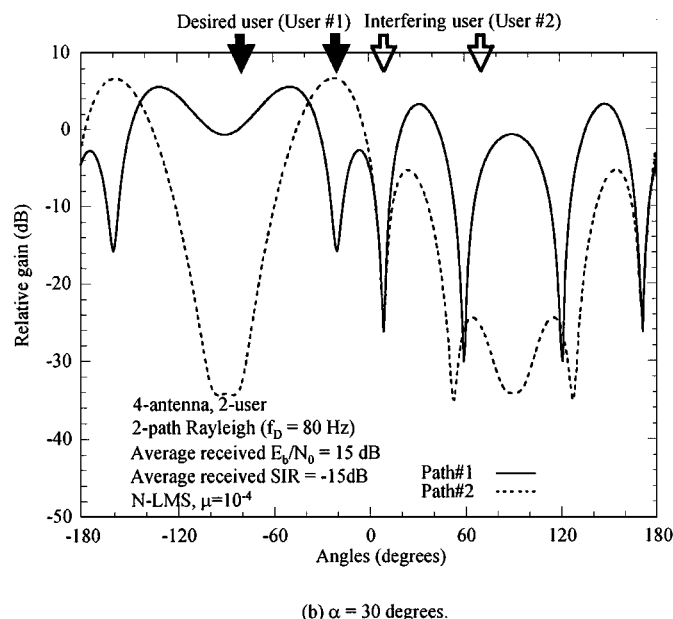
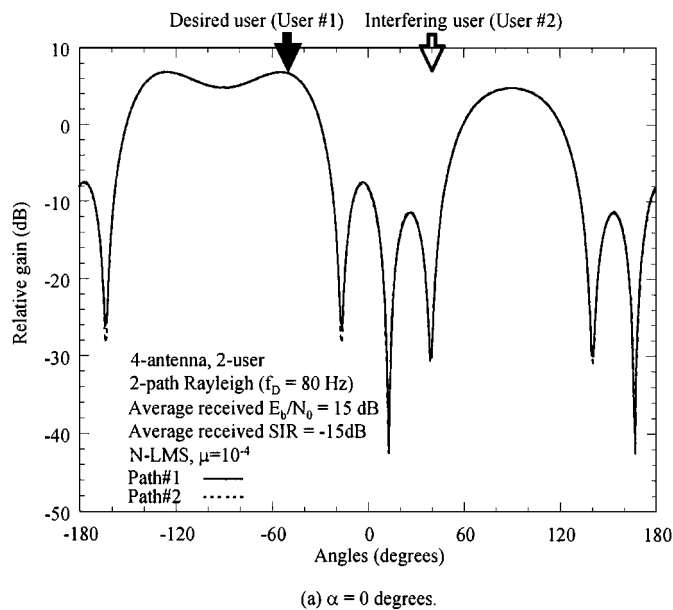


Fig. 3. Effect of angle spread of two-path DOA's on generated beam pattern. Laboratory experiment. (a)  $\alpha = 0^\circ$ . (b)  $\alpha = 30^\circ$ .

time delay (carrier phase difference) among the four RF cables were measured (their lengths were approximately 60 m and the amplitude differences were within 0.2 dB). The measured mutual couplings between array antennas were approximately -26 dB and can be neglected. Hence, its influence was not taken into account in the beam pattern computation.

The average total received signal energy per information bit-to-background power spectrum density ratio ( $E_b/N_0$ ) of User #1 was set to 15 dB, and the average received signal-to-interference power ratio (SIR) at each antenna of User #1 was set to -15 dB. Fig. 3(a) clearly shows that, when  $\alpha = 0$ , the beam former accurately forms the beam null toward the DOA of User #2; the direction error of the beam null is within  $3^\circ$ . When  $\alpha = 30^\circ$  [Fig. 3(b)], however, a beam null is also formed

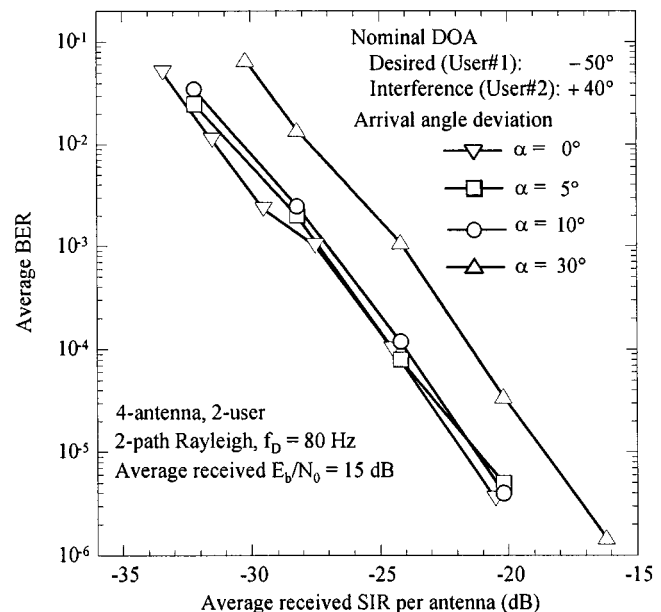


Fig. 4. Effect of angle spread of two-path DOA's on average BER performance. Laboratory experiment.

toward the DOA of the other path of User #1. When  $\alpha = 30^\circ$ , since the beam former generated all beam nulls toward the DOA's of the interfering signals (in our case, the freedom of the adaptive array which is equal to the maximum number of beam nulls was three), the depths of the beam nulls became shallower compared to the case with  $\alpha = 0^\circ$ . This resulted in degradation of the average BER performance.

The measured average BER performance when the nominal DOA's of the two users were similar to those in Fig. 3 is plotted in Fig. 4 as a function of the average received SIR at each antenna with  $\alpha$  as a parameter. Fig. 4 shows that almost the same BER performance is obtained for  $\alpha = 0-10^\circ$ , yet when  $\alpha = 30^\circ$ , as is indicated in Fig. 3(b), the BER performance degrades compared to that for  $\alpha = 0-10^\circ$  due to decreased null depths. Therefore, the degradation of error rates when  $\alpha = 0-10^\circ$  is not a serious problem. According to the propagation measurement, it was reported in [13] that  $\alpha$  is in the order of several degrees (i.e.,  $\alpha < 10^\circ$ ) for a high-elevation base station antenna and a long distance (e.g., an antenna height of 45 m and a distance of 3 km in downtown Tokyo), and in [16] that  $\alpha$  is within  $10^\circ$  with the probability of 80% with an antenna height of 70 m and a distance of 0.5–2 km in an urban area in Frankfurt. Therefore, it is understood that the PSA-CAAD receiver can sufficiently suppress interfering user signals for the practical values of  $\alpha$  ( $=0-10$ ) (of course the number of interfering users must be less than that of the antennas minus one).

To observe the impact of the average received SIR on the antenna beam, the generated beam pattern was measured for the average received SIR = 0, -5, -20 dB and the pattern is illustrated in Fig. 5. The DOA's of the two users are the same as those in Fig. 3 at each antenna with  $\alpha = 0^\circ$ . Fig. 5 shows that the beam null is accurately generated toward the DOA of the interfering user even for a large average received SIR such as 0 dB.

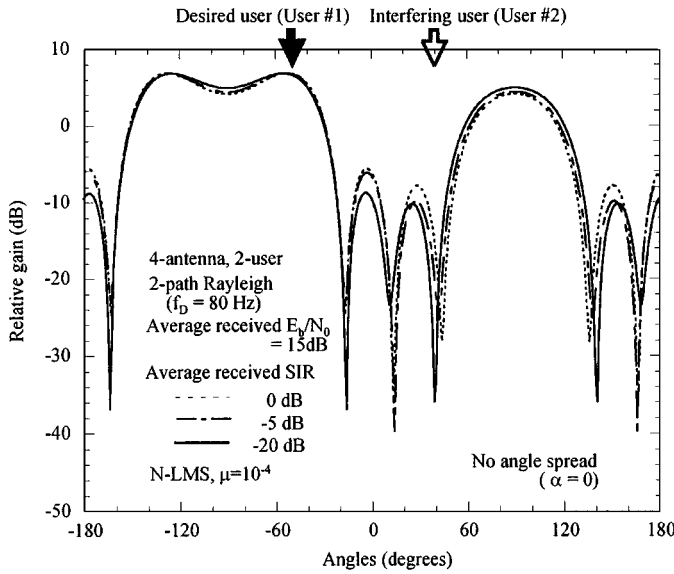


Fig. 5. Effect of average received SIR on generated beam pattern. Laboratory experiment.

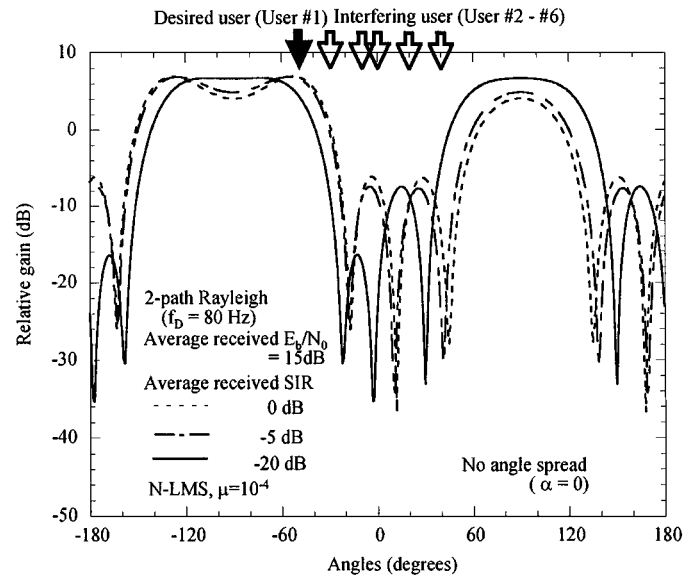


Fig. 7. Effect of average received SIR on generated beam pattern. Laboratory experiment.

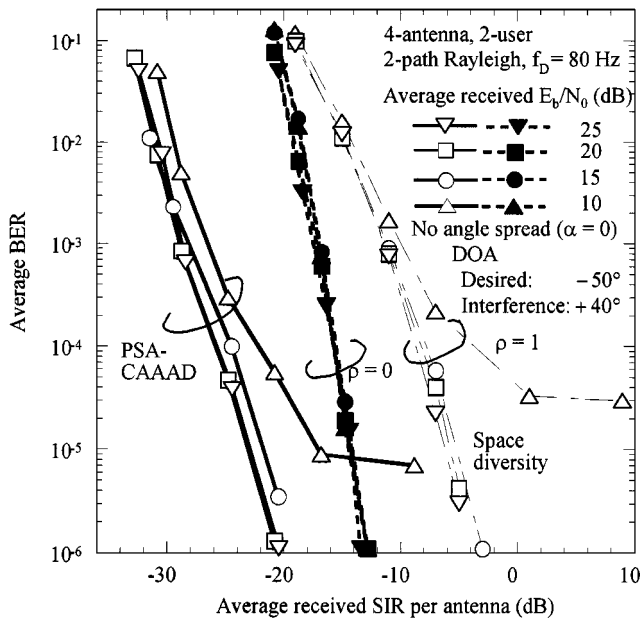


Fig. 6. Effect of average received  $E_b/N_0$  on average BER performance. Laboratory experiment.

The measured BER performance when the DOA's of the two users were similar to those in Fig. 3 with  $\alpha = 0^\circ$  is plotted in Fig. 6 with the average received  $E_b/N_0$  as a parameter. For comparison, the BER performance with a four-branch space diversity receiver using MRC is also shown, where the received signals of each resolved path on the four antennas were MRC combined and then Rake combined. For the space diversity receiver, two extreme cases of fading correlation,  $\rho = 0$  and 1.0 were considered. Apparently,  $\rho = 0$  achieved a better level of performance and therefore, in the following we compare the PSA-CAAAD receiver with space diversity receiver with  $\rho = 0$ . While the BER performance with the space diversity receiver is virtually insensitive to the average

received  $E_b/N_0$  value when the average received SIR  $< -10$  dB (in this SIR range, the channel is interference limited), the BER performance with the PSA-CAAAD receiver is sensitive to the average received  $E_b/N_0$  value. It was observed that with the PSA-CAAAD receiver, as the average received  $E_b/N_0$  value increased, the BER performance improved because of the increased depth of the beam nulls. This is because a more accurate reference signal can be generated due to the improved channel estimation, and because the interference power level was suppressed to as low as the background noise level due to the effect of beam forming. Even when the average received  $E_b/N_0 = 10$  dB, the PSA-CAAAD receiver achieved the average BER  $= 10^{-3}$  at the average received SIR  $= -26$  dB while the space diversity receiver required a 9-dB larger received SIR value. When the average received  $E_b/N_0$  was increased to 20 dB, the superiority of the PSA-CAAAD receiver to the space diversity receiver became more evident, and there was an additional reduction of approximately 2.5 dB in the required average received SIR. It should be noted that to obtain  $\rho = 0$ , the antenna spacing between two adjacent antennas must be wider than several carrier wavelengths at the base station [14], however, for the PSA-CAAAD receiver only a 0.5 carrier-wavelength antenna separation was required.

Until now, we assumed two-user environments (the number of interfering users is smaller than that of the beam nulls). Therefore, we also investigated the beam pattern and average BER performance when the number of interfering users is larger than that of the beam nulls. The beam patterns of a six-user environment (five-interfering user) are shown in Fig. 7 with the average received SIR of User #1 user as a parameter with  $\alpha = 0$ . The DOA's of User #1, #2, #3, #4, #5, and #6 were set to  $-50^\circ$ ,  $-30^\circ$ ,  $-10^\circ$ ,  $0^\circ$ ,  $+20^\circ$ , and  $+40^\circ$ , respectively. It was assumed that the average received  $E_b/N_0 = 15$  dB. The figure shows that as the average received SIR decreased, the antenna gain toward the DOA of the interference became smaller. Although the three beam nulls were not generated toward each

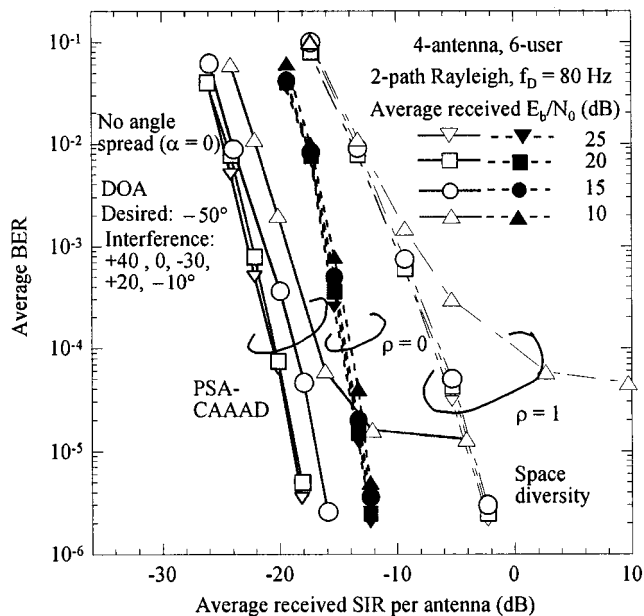


Fig. 8. Effect of average received  $E_b/N_0$  on average BER performance. Laboratory experiment.

DOA of the interfering user, the interference suppression of more than approximately 16 dB was obtained.

The measured average BER performance in a six-user environment as a function of the average received SIR at each antenna with  $\alpha = 0^\circ$  is shown in Fig. 8 with the average received  $E_b/N_0$  as a parameter when the DOA's of six users were the same as that in Fig. 7. The BER performance of four-branch space diversity receiver using MRC with  $\rho = 0$  was also plotted for comparison. Compared to the 2-user case in Fig. 6, the BER performance with space diversity reception was degraded by approximately 2 dB for the required received SIR. The degradation compared to the 2-user case with PSA-CAAAD reception becomes much larger than space diversity because the beam nulls are not generated toward the DOA's of interfering users. However, even when the number of interfering users is larger than that of the beam nulls, it is clear that the required average received SIR of the PSA-CAAAD receiver for achieving the average BER of  $10^{-3}$  can be reduced by approximately 6 dB compared to the MRC space diversity reception when the average received  $E_b/N_0 = 20$  dB.

The measured average BER performance with the number of multipaths  $L$  as a parameter in the six-user environment is plotted in Fig. 9 as a function of the average received SIR at each antenna. The DOA's of the six users are similar to those in Fig. 7 with  $\alpha = 0^\circ$ . The figure shows that the PSA-CAAAD is superior to space diversity reception with  $\rho = 0$  except for  $L = 1$ . This implies that the Rake receiver worked satisfactorily so that the instantaneous SINR was maximized. For  $L = 1$ , the BER performance of the PSA-CAAAD was worse than that of space diversity when the average received SIR was larger than  $-14$  dB. In this case, the impact of the background noise was dominant compared to the interference, and hence the space diversity was more effective. When  $L = 3$ , the BER performance improved most with PSA-CAAAD receiver or space diversity due to the Rake time diversity effect.

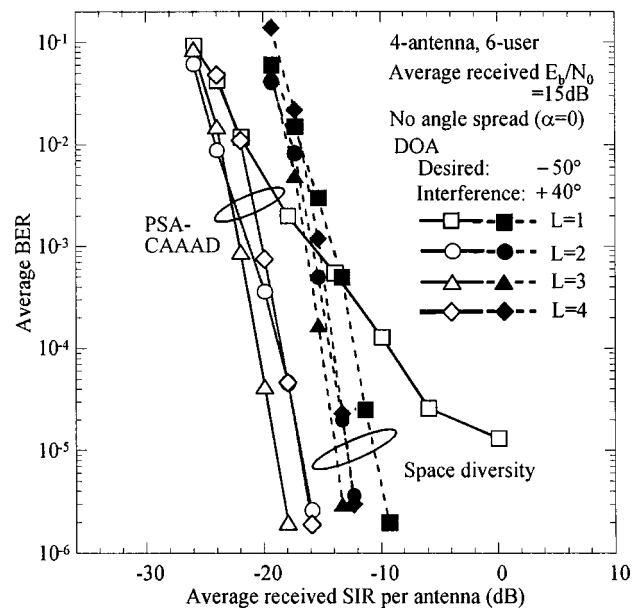


Fig. 9. Effect of the number of multipath on average BER performance. Laboratory experiment.

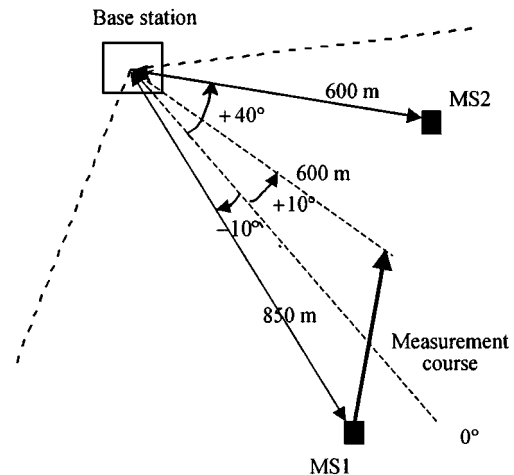
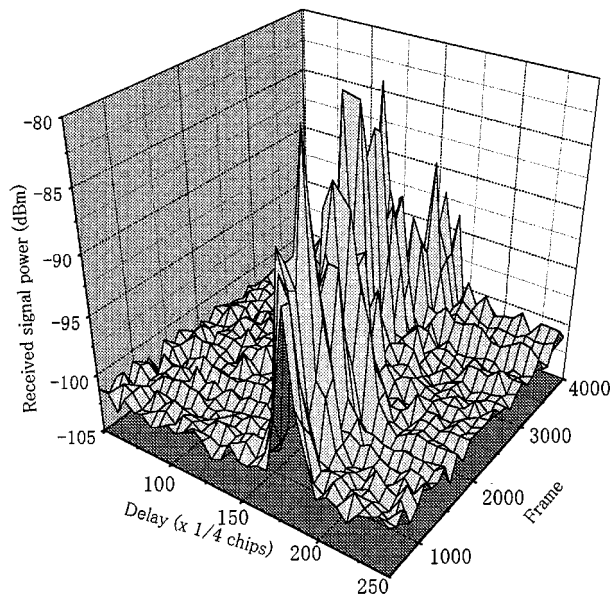


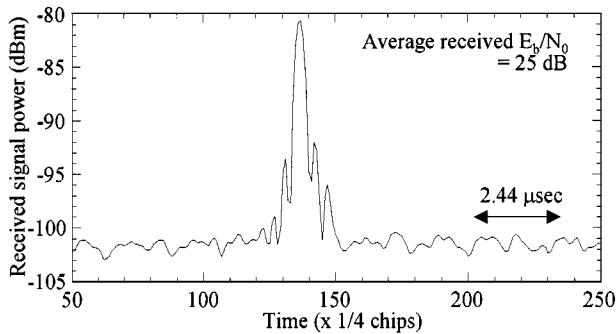
Fig. 10. Measurement course for field experiment.

#### IV. FIELD EXPERIMENTS

Field experiments were conducted in an area nearby Tokyo in two-user environment (hereafter we denote the desired and interfering users as MS1 and MS2, respectively). The antenna heights of the base station and the mobile stations were 50 and 2.9 m from the ground, respectively. The measurement course is illustrated in Fig. 10. We measured the beam pattern and BER performance when MS1 equipped with a mobile transceiver was driven along the measurement courses at an average speed of approximately 30 km/h and MS2 was stationary at a fixed location. The distances of MS1 and MS2 from the base station were 600–850 and 600 m, respectively. In the measurement course, the look angle from the base station changed from  $-10^\circ$  to  $+10^\circ$  and MS2 was stationary at the look angle of  $+40^\circ$ . Therefore, the angle difference between MS1 and MS2 varied from 50 to  $30^\circ$ . The measured power delay profile in the measurement course is also plotted in Fig. 11. A residential apartment



(a)



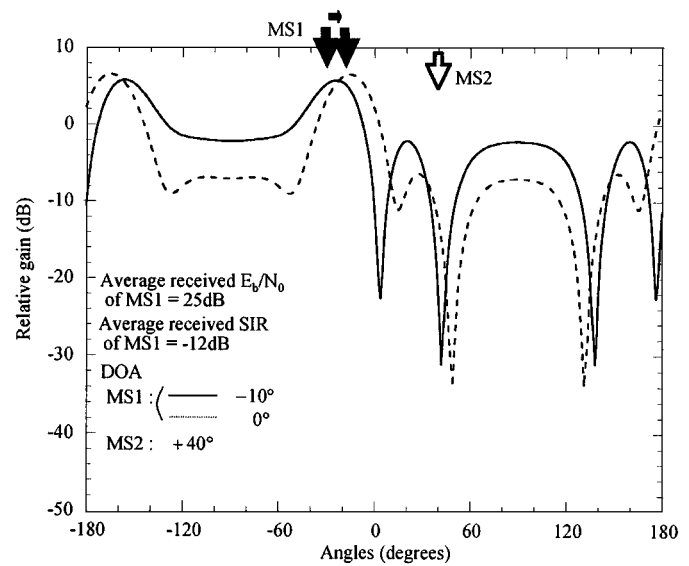
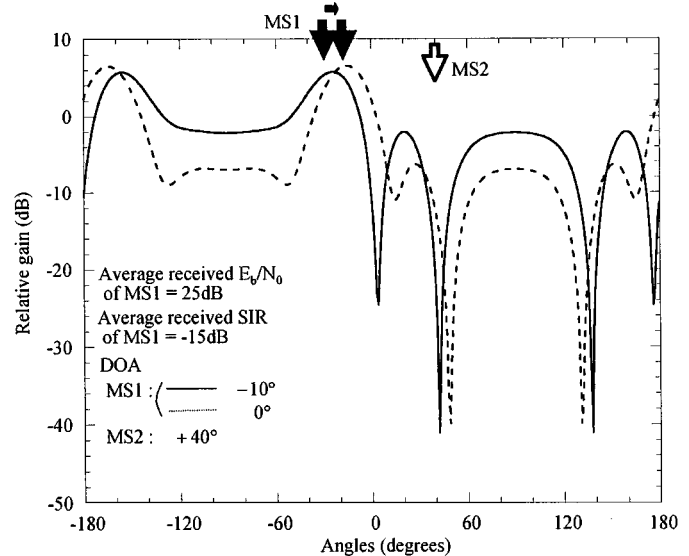
(b)

Fig. 11. Measured power delay profiles. (a) MS1. (b) MS2.

building and an office building were located along the measurement course, resulting in one-to-two path fading appearing in the first half of the course, followed by two-to-three path fading with an average power difference of approximately 3 dB, while MS2 was almost in the line-of-sight path (thus, a single path).

The generated beam pattern associated with one of two resolved paths of MS1 is plotted in Fig. 12 for the average received  $E_b/N_0$  of MS1 of 25 dB. The figure shows that the direction of the main lobe shifts along with the movement of MS1. Although MS2 is located at the fixed point at  $+40^\circ$ , the directions of the beam nulls are also shifted according to the movement of MS1. This is because the receiver antenna weights are updated to enhance the gain toward the DOA of MS1 in order to maximize the received SIR after weight combining. The depth when the average received SIR =  $-15$  dB is larger than that of average received SIR =  $-12$  dB.

The measured BER performance is plotted in Fig. 13 as a function of the average received signal power with the average received SIR of MS1 as a parameter. The average received  $E_b/N_0$  of the MS1 was set to 25 dB. For comparison, the results of the MRC space diversity receiver are also plotted (antenna separation was  $10 \lambda$ ). The laboratory experimental results using a 2-path average equal channel model with  $f_D = 80$  Hz are also plotted. The figure shows the required received

(a) Average received SIR =  $-12$  dB(b) Average received SIR =  $-15$  dBFig. 12. Generated beam patterns. Field experiment. (a) Average received SIR =  $-12$  dB. (b) Average received SIR =  $-15$  dB.

signal power with the PSA-CAAAD receiver can be decreased by approximately 5–10 dB and 8–10 dB compared to MRC space diversity reception for the average received SIR =  $-12$  and  $-15$  dB, respectively. This is because the beam nulls are formed toward the DOA of MS2 with a high transmit power. In space diversity reception, the required received signal power of the field results at the average BER of  $10^{-3}$  increases by approximately 1–4 dB compared to the laboratory experimental results. This degradation is considered to be due to the path search error for Rake combining and to the fact that the channel model assumed in the laboratory experiment does not exactly represent the real channel. The degradation of field results from the laboratory experiments with the PSA-CAAAD receiver becomes larger than that with space diversity reception due to

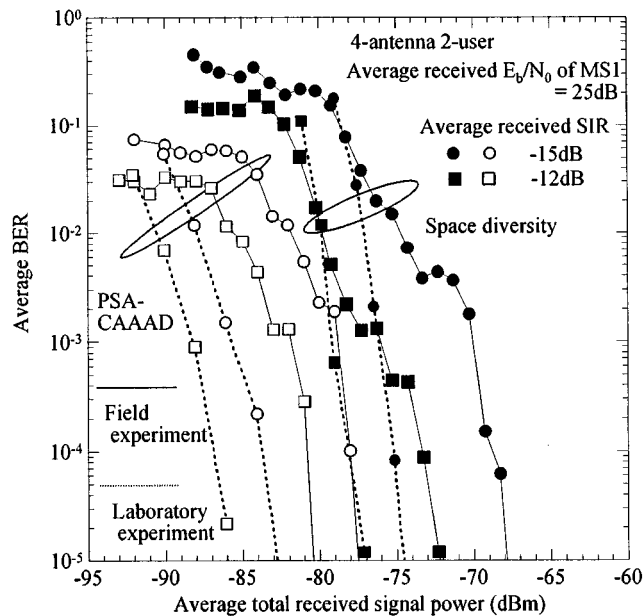


Fig. 13. Average BER performance as a function of average total received signal power. Field experiment.

the increased path search error since the received signal power is much lower.

## V. CONCLUSION

A four-antenna PSA-CAAAD receiver was implemented and its performance in a fading environment was evaluated by both laboratory and field experiments assuming two users. Its important design concept is that the beam former forms the antenna beam for each resolved propagation path based on the MMSE criterion, but does not require tracking of fast fading (this is the task of the subsequent Rake combiner). This paper conclusively showed that the beam nulls can be formed toward the DOA's of the interfering user paths even under severe interference limited conditions (i.e., the average received SIR < -10 dB). Although the beam null depth becomes shallower as the average received  $E_b/N_0$  decreases, the average BER performance is still better than that of the space diversity receiver even when the average received  $E_b/N_0$  is as low as 10 dB; the gain from the space diversity receiver is 9 (3.5) dB at the average BER =  $10^{-3}$  for 2-user (6-user) environment [1(5)-interfering user(s)]. Furthermore, the PSA-CAAAD receiver is more compact; total antenna separation is only  $1.5 \lambda$  for the four-antenna PSA-CAAAD receiver, while it is at least several times carrier wave length for the space diversity receiver to achieve sufficiently low fading correlation.

In the field experiment, it was confirmed that the antenna beam nulls can be formed toward the interfering user and that the average BER performance was improved over that of the space diversity receiver in 2 user environments where the desired user traveled at a average speed of approximately 30 km/h. The direction error of the formed beam null was larger (about  $7^\circ$ ) than the laboratory experiment (about  $3^\circ$ ) and the required received signal power with the PSA-CAAAD receiver can be decreased by approximately 5–10 dB and 8–10 dB compared to MRC

space diversity reception for the average received SIR = -12 and -15 dB, respectively.

Through the laboratory and field experiments, we demonstrated the high potential of the PSA-CAAAD receiver to significantly reduce MAI from high rate users compared to the space diversity receiver.

## REFERENCES

- [1] F. Adachi, M. Sawahashi, and H. Suda, "Wideband DS-CDMA for next generation mobile communications system," *IEEE Commun. Mag.*, vol. 36, pp. 56–69, Sept. 1998.
- [2] E. Dahlman, B. Gudmundson, M. Nilsson, and J. Skold, "UMTS/IMT-2000 based on wideband CDMA," *IEEE Commun. Mag.*, vol. 36, pp. 70–80, Sept. 1998.
- [3] "Special issue, IMT-2000: Standards efforts of the ITU," *IEEE Personal Commun.*, vol. 4, Aug. 1997.
- [4] R. T. Compton Jr., "An adaptive antenna in a spread-spectrum communication system," *Proc. IEEE*, vol. 66, pp. 289–295, March 1978.
- [5] S. C. Swales, M. A. Beach, D. J. Edwards, and J. P. McGeehan, "The performance enhancement of multibeam adaptive base-station antennas for cellular land mobile radio systems," *IEEE Trans. Veh. Technol.*, vol. 39, pp. 56–67, Feb. 1990.
- [6] G. V. Tsoulos, M. A. Beach, and S. C. Swales, "Performance enhancement of DS-CDMA microcellular networks with adaptive antennas," in *Proc. 46th IEEE Veh. Technol. Conf.*, Atlanta, U.S.A., April 28–May 1 1996, pp. 1086–1090.
- [7] H. Wang, R. Kohno, and H. Imai, "Adaptive array antenna combined with tapped delay line using processing gain for direct-sequence/spread-spectrum multiple access system," *IEICE Trans. Commun.*, vol. J75-B-II, pp. 815–825, Nov. 1992.
- [8] Y. Wang and J. R. Cruz, "Adaptive antenna arrays for the reverse link of CDMA cellular communication systems," *Electron. Lett.*, vol. 30, pp. 1017–1018, June 1994.
- [9] T. Ohgane, "Spectral efficiency improvement by base station antenna pattern control for mobile cellular systems," *IEICE Trans. Commun.*, vol. E77-B, pp. 598–605, May 1994.
- [10] S. Tanaka, M. Sawahashi, and F. Adachi, "Pilot symbol-assisted decision-directed coherent adaptive array diversity for DS-CDMA mobile radio reverse link," *IEICE Trans. Fundamentals*, vol. E80-A, pp. 2445–2454, Dec. 1997.
- [11] S. Haykin, *Adaptive Filter Theory*. Englewood Cliffs, NJ: Prentice-Hall, 1991.
- [12] Y. Honda and K. Jamal, "Channel estimation based on time-multiplexed pilot symbols," *IEICE Tech. Rep.*, RCS96-70, Aug. 1996.
- [13] S. Kozono and S. Sakagami, "Correlation coefficient on base station diversity for land mobile communication system," *IEICE Trans. Commun.*, vol. J70-B, pp. 476–482, Apr. 1987.
- [14] F. Adachi, M. T. Feeney, A. G. Williamson, and J. D. Parsons, "Cross-correlation between the envelopes of 900 MHz signals received at a mobile radio base-station site," *Proc. IEE*, pt. F, vol. 133, pp. 506–512, Oct. 1986.
- [15] F. Adachi, M. Sawahashi, and H. Suda, "Wideband DS-CDMA for next generation mobile communication system," *IEEE Commun. Mag.*, vol. 36, pp. 56–69, Sept. 1998.
- [16] U. Martin, "Spatio-temporal radio channel characteristics in urban macrocells," *IEE Proc.-Radar, Sonar Navig.*, vol. 145, Feb. 1998.
- [17] J. H. Winters, "Optimal combining in digital mobile radio with co-channel interference," *IEEE Trans. Veh. Technol.*, vol. VT-33, pp. 144–155, Aug. 1984.
- [18] "Specifications of Air-Interface for 3G Mobile System Ver. 0.0," Assoc. Radio Ind. Businesses (ARIB), Dec. 18, 1997.
- [19] 3GPP RAN 25.211 V3.1.0, Dec. 1999.
- [20] J. Litva and T. K. Lo, *Digital Beamforming in Wireless Communications*. Boston, MA: Artech House, 1996.

**Shinya Tanaka** received the B.S. degree from Waseda University, Tokyo, Japan in 1993. In 1993 he joined NTT Mobile Communication Network, Inc. (NTT DoCoMo). Since joining NTT DoCoMo, he has been engaged in the research and development of adaptive antenna array for DS-CDMA. He is a Member of the Institute of Electronics, Information, and Communication Engineers of Japan.

**Atsushi Harada** received the B.S. and M.S. degrees from Kyushu University, Fukuoka, Japan in 1996 and 1998, respectively. In 1998, he joined NTT Mobile Communication Network, Inc. (NTT DoCoMo). Since joining NTT DoCoMo, he has been engaged in the research and development of adaptive antenna array for DS-CDMA. He is a Member of the Institute of Electronics, Information, and Communication Engineers of Japan.



**Mamoru Sawahashi** (M'88) received the B.S. and M.S. degrees from Tokyo University in 1983 and 1985, respectively, and received the Dr. Eng. Degree from Nara Institute of Technology in 1998. In 1985 he joined NTT Electrical Communications Laboratories, and in 1992 he transferred to NTT Mobile Communications Network, Inc. (now NTT DoCoMo, Inc.). Since joining NTT, he has been engaged in the research of modulation/demodulation techniques for mobile radio, and research and development of wireless access technologies for

W-CDMA mobile radio and broadband wireless packet access technologies for beyond IMT-2000. He is now a Director of Wireless Access Laboratory of NTT DoCoMo, Inc.



**Fumiyuki Adachi** (M'79-SM'90) received the B.S. and Dr. Eng. degrees in electrical engineering from Tohoku University, Sendai, Japan, in 1973 and 1984, respectively. In 1973, he joined the Electrical Communications Laboratories of Nippon Telegraph & Telephone Corporation (now, NTT) and conducted various research related to digital cellular mobile communications. From July 1992 to December 1999, he was with NTT Mobile Communications Network, Inc., where he led a research group on wideband/broadband CDMA

wireless access for IMT-2000 and beyond. Since January 2000, he has been with the Graduate School of Engineering, Tohoku University, where he is a Professor of communications engineering. His research interests include: CDMA and TDMA wireless access techniques, CDMA spreading code design, Rake receiver, transmit/receive antenna diversity, adaptive antenna array, bandwidth-efficient digital modulation, and channel coding. From October 1984 to September 1985, he was a United Kingdom SERC Visiting Research Fellow in the Department of Electrical Engineering and Electronics at Liverpool University. From April 1997 to March 2000, he was a Visiting Professor at Nara Institute of Science and Technology, Japan. He has written chapters of three books: Y. Okumura and M. Shinji Eds., *Fundamentals of Mobile Communications* published in Japanese by IEICE, 1986; M. Shinji, Ed., *Mobile Communications* published in Japanese by Maruzen Publishing Co., 1989; and M. Kuwabara ed., *Digital Mobile Communications* published in Japanese by Kagaku Shinbun-sha, 1992. He was a Co-Recipient of the IEEE Vehicular Technology Transactions best paper of the year award 1980 and again 1990. He is a Member of IEICE of Japan and was a co-recipient of the IEICE Transactions best paper of the year award 1996 and again 1998.